npj | climate and atmospheric science

www.nature.com/npjclimatsci

ARTICLE OPEN

Check for updates

Understanding climate change impacts on drought in China over the 21st century: a multi-model assessment from CMIP6

Feng Xu[1,10], Yanping Qu[2,10], Virgílio A. Bento[3], Hongquan Song[4], Jianxiu Qiu[5], Junyu Qi[6], Lingling Wan[1], Rongrong Zhang[1], Lijuan Miao[7], Xuesong Zhang[8] and Qianfeng Wang[1,9]✉

The future state of drought in China under climate change remains uncertain. This study investigates drought events, focusing on the region of China, using simulations from five global climate models (GCMs) under three Shared Socioeconomic Pathways (SSP1-2.6, SSP3-7.0, and SSP5-8.5) participating in the Inter-Sectoral Impact Model Intercomparison Project (ISIMIP3b). The daily Standardized Precipitation Evapotranspiration Index (SPEI) is employed to analyze drought severity, duration, and frequency over three future periods. Evaluation of the GCMs' simulations against observational data indicates their effectiveness in capturing historical climatic change across China. The rapid increase in CO_2 concentration under high-emission scenarios in the mid- and late-future century (2040–2070 and 2071–2100) substantially influences vegetation behavior via regulation on leaf stomata and canopy structure. This regulation decelerates the increase in potential evapotranspiration, thereby mitigating the sharp rise in future drought occurrences in China. These findings offer valuable insights for policymakers and stakeholders to develop strategies and measures for mitigating and adapting to future drought conditions in China.

npj Climate and Atmospheric Science (2024)7:32 ; https://doi.org/10.1038/s41612-024-00578-5

INTRODUCTION

Drought, a phenomenon that occurs globally, is a widespread natural disaster known for being among the most damaging and economically challenging of all natural events. Its effects can be disastrous for agriculture, the economy, and society at large[1–3]. In the 21st century, the estimated annual economic loss caused by drought ranges between $6 billion and $8 billion, surpassing any other climate disaster[4–7]. In China, drought also represents a major natural disaster, causing significant socioeconomic losses, particularly in the agriculture sector[8–10]. From the 1950s to the early 21st century, there has been a notable rise in the average annual crop yield losses due to drought, escalating from 4.35 to 34.9 million tons[11]. Thus, understanding the anticipated changes in drought is crucial for developing prompt early warning and mitigation policies.

Effective drought indices are crucial for the monitoring and evaluation of drought. There are multiple indices available that offer diverse perspectives in characterizing drought conditions[4,8,12,13]. Commonly used indices include the Palmer Drought Severity Index (PDSI), the self-calibrating Palmer Drought Severity Index (scPDSI), and the Standardized Precipitation Index (SPI)[14–16]. However, the PDSI and scPDSI have issues with fixed timescales, inadequate data-related calibration, and limited spatial comparability[17]. While the SPI can detect and evaluate drought at various scales, it accounts solely for precipitation and neglects the impacts of other meteorological factors such as evapotranspiration[18]. By integrating the strengths of PDSI and SPI, the Standardized Precipitation Evapotranspiration Index (SPEI) offers a comprehensive approach to drought characterization[19,20]. It possesses the capacity to recognize droughts at various timescales as well as accounting for the influence of evapotranspiration on drought[20]. Consequently, SPEI represents a superior tool for investigating the progression of dryness under future climate change.

The SPEI is extensively used for drought monitoring and characterization. Nonetheless, prior research has often depended on monthly SPEI, which comes with its own set of inherent limitations[21]. Even several days of drought can have serious consequences during the critical period of vegetation growth[22–24]. Since the monthly SPEI cannot identify droughts lasting less than 1 month, it tends to overlook the impacts of short and sudden droughts, such as flash drought[20]. Therefore, the recent development of the daily SPEI effectively addresses this research gap[22,25]. The calculation and application of the daily SPEI follow a similar approach to that of the monthly SPEI[19,20]. It facilitates drought monitoring and assessment across various timescales, enabling precise identification of drought onset and cessation dates, along with the duration of drought events[22,26]. Unlike the monthly SPEI commonly utilized in past research, the daily SPEI more accurately detects short-term drought events, enhancing the accuracy of drought monitoring and assessment[20,21]. Therefore, the use of the daily SPEI emerges as a more advantageous approach.

Conventional models used for calculating potential evapotranspiration (PET), which do not take into account the effects of CO_2 on vegetation, could result in an overestimation of future PET and drought conditions. Two widely used Penman-Monteith models include the open-water Penman model (Penman-ow)[27] and the

[1]Fujian Provincial Key Laboratory of Remote Sensing of Soil Erosion and Disaster Protection/College of Environmental & Safety Engineering, Fuzhou University, 350116 Fuzhou, China. [2]Research Center on Flood and Drought Disaster Reduction, China Institute of Water Resources and Hydropower Research, 100038 Beijing, China. [3]University of Lisbon, Faculty of Sciences, Instituto Dom Luiz, Lisbon, Portugal. [4]College of Geography and Environmental Science, Henan University, 475004 Kaifeng, China. [5]Guangdong Provincial Key Laboratory of Urbanization and Geo-simulation, School of Geography and Planning, Sun Yat-sen University, 510275 Guangzhou, China. [6]Earth System Science Interdisciplinary Center, University of Maryland, College Park, 5825 University Research Court, College Park, MD 20740, USA. [7]School of Geographical Sciences, Nanjing University of Information Science and Technology, 210044 Nanjing, China. [8]USDA-ARS Hydrology and Remote Sensing Laboratory Building 007, Room 104, BARC-West, Beltsville, MD 20705-2350, USA. [9]Key Lab of Spatial Data Mining & Information Sharing, Ministry of Education of China, 350116 Fuzhou, China. [10]These authors contributed equally: Feng Xu, Yanping Qu. ✉email: wangqianfeng@fzu.edu.cn

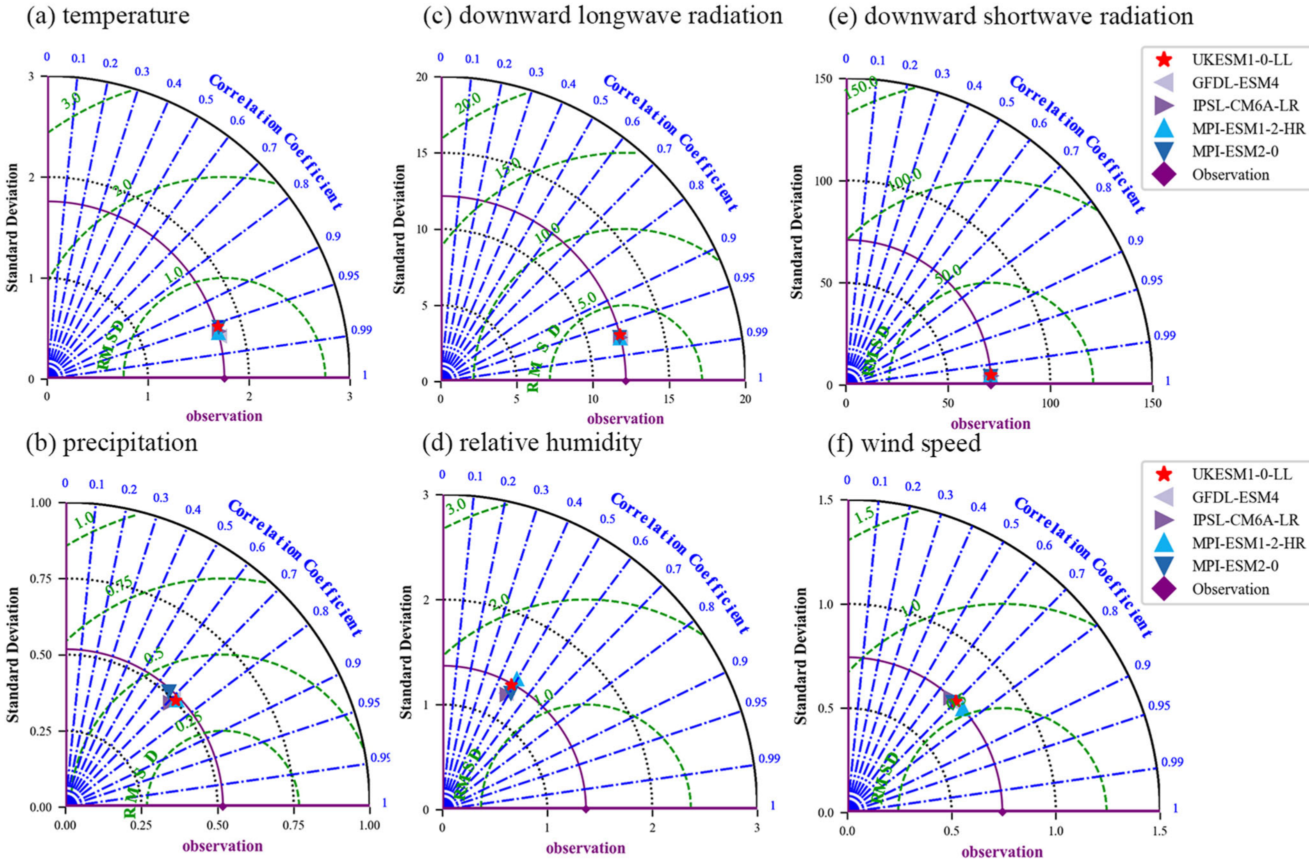

Fig. 1 Taylor diagrams for climate variables across China (1980-2014). Taylor diagrams of simulated **a** temperature, **b** precipitation, **c** downward longwave radiation, **d** relative humidity, **e** downward shortwave radiation, and **f** wind speed by 5 GCMs across China for the period of 1980–2014 against observed data. The dashed green line is the root mean square deviation (RMSD).

reference crop Penman-Monteith model (PM-RC)[28]. While these models fully account for the impact of radiative and aerodynamic components, they ignore the response of vegetation to climate change. Particularly, they do not consider the effects of CO_2, which may result in an overestimation of PET and future droughts[29–31]. Recognizing this limitation, Yang[32] proposed a method that considers changes in surface resistance to atmospheric CO_2 uptake in a warming climate within the Penman-Monteith method (PM-CO_2). This approach addresses the problem of conventional models overlooking the impact of CO_2 on vegetation. Consequently, the PM-CO_2 model offers a more comprehensive evaluation of future drought conditions in China.

The most advanced GCMs within the Coupled Model Intercomparison Project Phase 6 (CMIP6) present significant opportunities for improving the prediction capabilities of future drought. GCMs from CMIP6 have been extensively employed in previous research[33–37], and have demonstrated their robust capacities to capture drought characteristics[18,36,38]. Many research projects have used CMIP6 to forecast droughts on both global and regional scales. These studies generally indicate a trend toward more severe droughts in most areas, with China notably identified as a hotspot for these intensified conditions[2,17,39,40]. CMIP6, with its enhanced resolution and more extensive range of parameters, has demonstrated improved capabilities in simulating temperature and precipitation patterns[34,41–45]. Furthermore, CMIP6 has incorporated the representative concentration pathways into shared social economic pathways (SSPs), making it well-suited for future climate change research and drought prediction in China[46,47].

In this study, we used the enhanced PET model to calculate daily SPEI for assessing potential changes in meteorological droughts across China. We selected five GCMs from the Inter-Sectoral Impact Model Intercomparison Project (ISIMIP3b) to analyze and evaluate the characteristics of drought in China over three future periods: the early (2015–2040), middle (2041–2070), and late (2071–2100) 21st century. Furthermore, we examined the efficacy of these five GCMs in predicting future droughts under three extreme scenarios (SSP1-2.6, SSP3-7.0, and SSP5-8.5). This study presents state-of-the-art research into the future of drought events in China, by using the daily SPEI. It not only offers valuable insights into the potential changes in drought patterns but also establishes methodological frameworks for future drought research in China.

RESULTS

Model performance evaluation

Although bias-adjusted data from the ISIMIP3b GCMs are widely documented as being suitable for various global regions[48,49], it is still essential to evaluate the performance of simulations conducted by these five GCMs within our specific study area. The assessment results (Fig. 1) demonstrate that the simulated climate variables from the five GCMs, after bias adjustment, align well with the measurements (W5E5 v2.0), particularly for meteorological factors such as temperature and radiation. This result indicates that the chosen GCMs possess a robust capability to accurately represent climate change in China. As such, using these five GCMs to explore future drought conditions in the region is a viable approach.

Projected changes in key climate variables

The analysis of the time series for crucial climate variables spanning from 2015 to 2100 (Fig. 2) reveals that under the high-

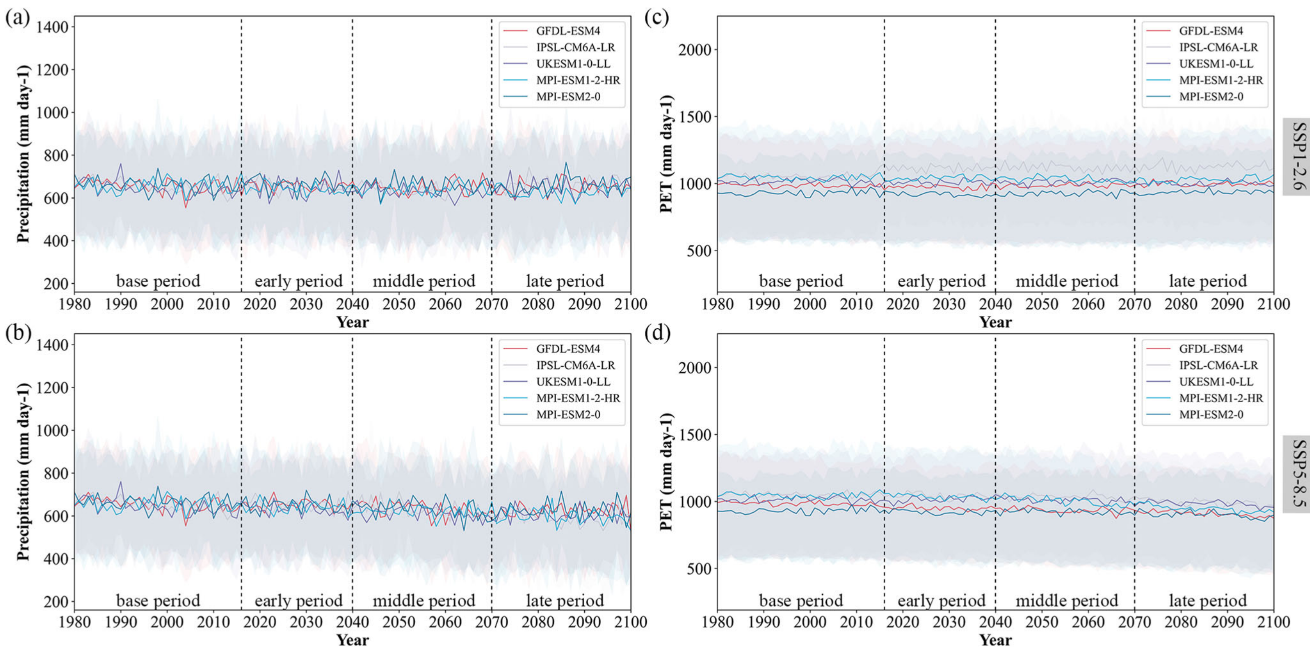

Fig. 2 Time series of precipitation and PET under different scenarios. Time series of precipitation under **a** SSP1-2.6 and **b** SSP5-8.5, PET calculated from PM-CO2 under **c** SSP1-2.6 and **d** SSP5-8.5 by five GCMs. The solid line represents the annual mean of all global grids, while the shades represent the lower (25th percentile) and upper limits (75th percentile).

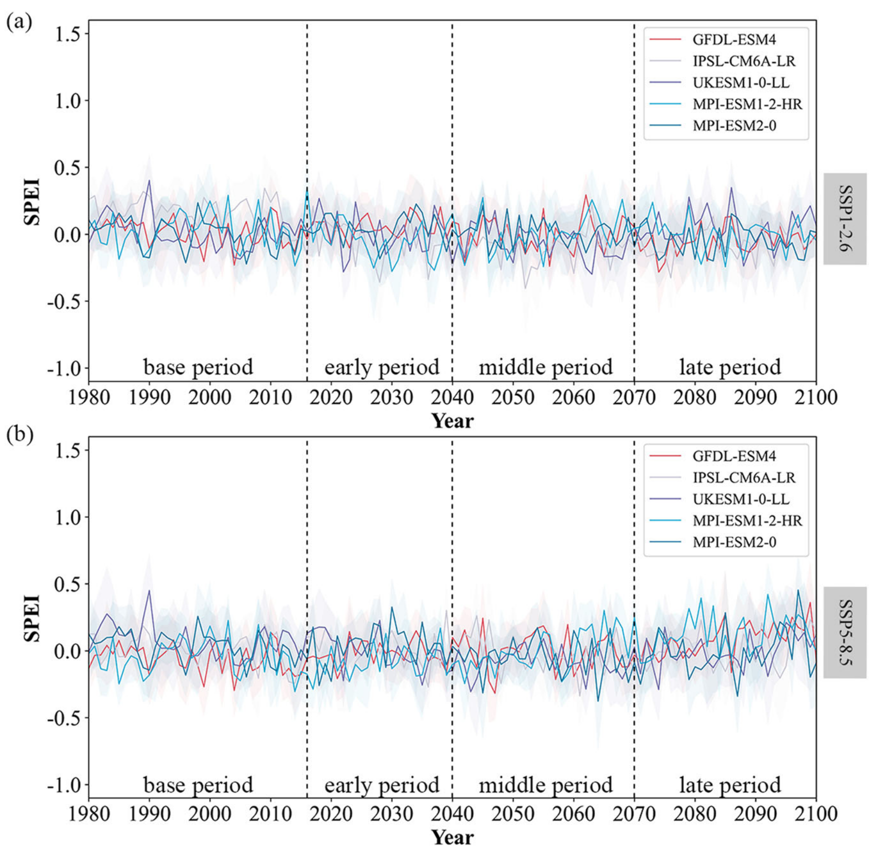

Fig. 3 Interannual variation of daily SPEI under different scenarios. Interannual variation of daily SPEI (PET calculated from PM-CO2) under **a** SSP1-2.6 and **b** SSP5-8.5. The solid line represents the annual mean of all global grids, while the shades represent the lower (25th percentile) and upper limits (75th percentile).

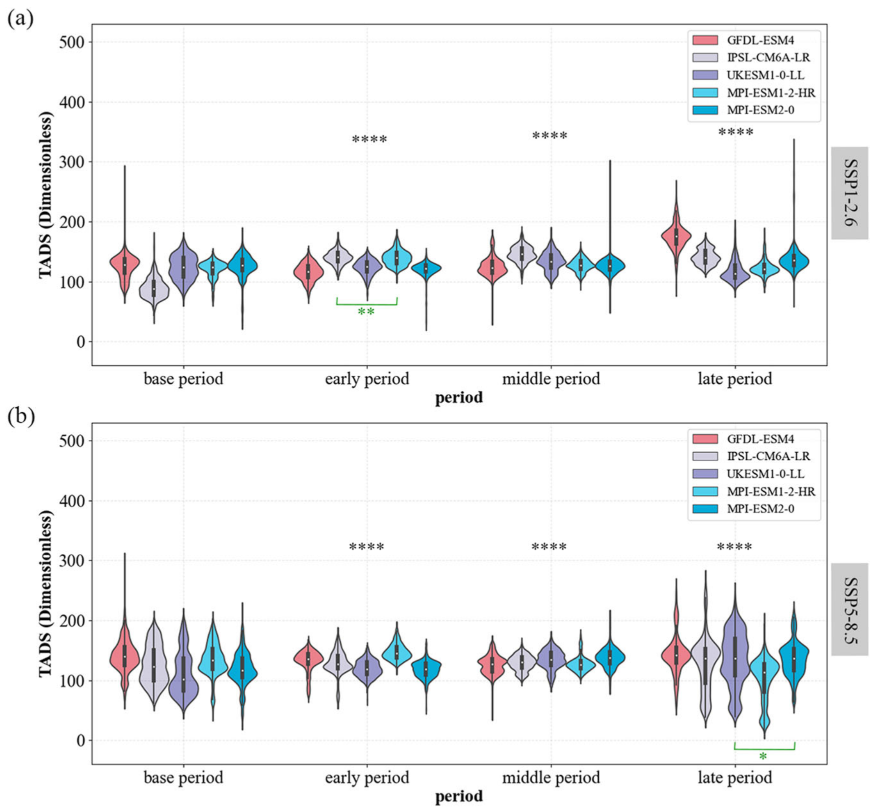

Fig. 4 Total annual drought severity under different scenarios and time periods. TADS (PET calculated from PM-CO2) for the base period (1980–2014) and three future periods (2015–2040, 2041–2070, and 2071–2100) under **a** SSP1-2.6 and **b** SSP5-8.5. Significance levels are indicated by **** for $p \leq 0.0001$, *** for $p \leq 0.001$, ** for $p \leq 0.01$, and * for $p \leq 0.05$. The lower green sign indicates the p-value between two GCMs, and the upper **** sign represents that the p-value between all two GCMs, except the lower green one, is ≤0.0001.

emission scenario, there is a more pronounced reduction in precipitation and PET compared to the low-emission scenario. Additionally, this decrease becomes progressively more intense from the early through the middle to the late period. The rainfall predictions generated by the five GCMs display significant consistency across both the low and high-emission scenarios. For the SSP1-2.6 scenario, the IPSL-CM6A-LR model simulated the highest PET values, whereas the MPI-ESM2-0 model simulated the lowest. Similarly, under the SSP5-8.5 scenario, the PET values simulated by MPI-ESM2-0 were also on the lower side. Analyzing PET values from different methods (Fig. 2 and Supplementary Fig. 1) shows that under the SSP1-2.6 scenario, PET computed using both methods were almost the same. In contrast, under the SSP5-8.5 scenario, the conventional PM-RC method estimated higher PET with a noticeable increasing trend, whereas the PM-CO_2 method estimated lower PET, showing a declining trend in the middle and late periods. This discrepancy is mainly attributed to the swift rise in CO_2 concentrations (Supplementary Fig. 2) under the high-emission scenario. This increase in CO_2 significantly influenced vegetation behavior, leading to a slowed growth rate of PET.

Projected changes in daily SPEI

By examining the SPEI series from 2015 to 2100 (Fig. 3), we observed that under the SSP1-2.6 scenario, daily SPEI shows a slight decreasing trend. Conversely, under the SSP5-8.5 scenario, daily SPEI displays a fluctuating upward trend, particularly in the late 21st century, with a notable increase. When comparing SPEI derived from different methodologies (Fig. 3 and Supplementary Fig. 3), it's evident that under SSP1-2.6, the SPEI values calculated by both methods are almost the same. However, under SSP5-8.5, the SPEI values calculated using the conventional PM-RC method show a significant decline, particularly in the middle and late periods.

Projected changes in drought event characteristics

The total annual drought severity (TADS) is an important metric for assessing drought severity. Figure 4 illustrates TADS during the baseline period and over three future periods under two scenarios. In the future projections, the TADS values projected by GFDL-ESM4 and MPI-ESM2-0 increase, with a more pronounced change under the SSP1-2.6 scenario. Conversely, the TADS values projected by MPI-ESM1-2-HR exhibit a decline, whereas those by IPSL-CM6A-LR and UKESM1-0-LL remain relatively stable. Overall, there is no significant shift in drought severity across the three future periods. Pairwise comparisons of the five GCMs' TADS projections for the future three periods revealed statistically significant differences ($p < 0.05$). The comparison of drought severity as simulated by the two methods for PET (Fig. 4 and Supplementary Fig. 4) suggests minimal difference in drought severity between the baseline, early, and middle periods. However, in the late period, particularly under the SSP5-8.5 scenario, the drought severity simulated by the conventional PM-RC method is significantly higher than that of the method considering vegetation-CO_2 interaction.

The total annual drought duration (TADD) illustrates the extent of drought durations. Figure 5 displays the TADD values during the base period and over three future periods under two scenarios. In future projections, TADD projected by GFDL-ESM4 becomes longer under SSP1-2.6 and shorter under SSP5-8.5. MPI-ESM2-0 projects a longer TADD in the future, with more pronounced changes in SSP1-2.6. In contrast, future TADD

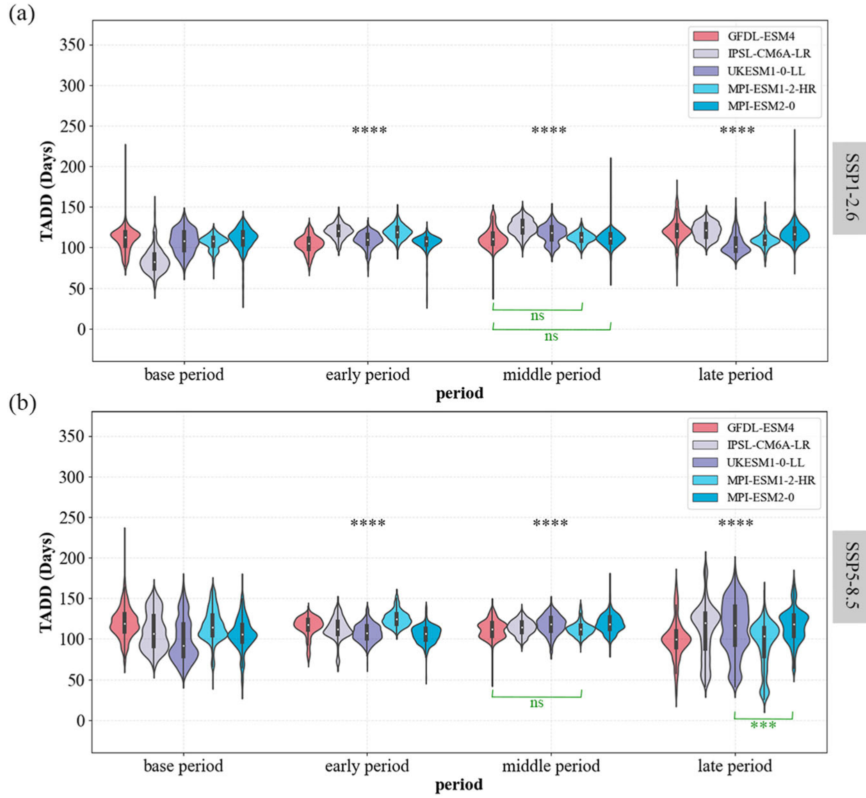

Fig. 5 Total annual drought duration under different scenarios and time periods. TADD (PET calculated from PM-CO2) for the base period (1980–2014) and three future periods (2015–2040, 2041–2070, and 2071–2100) under **a** SSP1-2.6 and **b** SSP5-8.5. Significance levels are indicated by **** for $p \leq 0.0001$, *** for $p \leq 0.001$, ** for $p \leq 0.01$, and * for $p \leq 0.05$. The lower green sign indicates the p-value between two GCMs, and the upper **** sign represents that the p-value between all two GCMs, except the lower green one, is ≤0.0001.

projected by MPI-ESM1-2-HR becomes shorter in both scenarios. TADD projected by IPSL-CM6A-LR and UKESM1-0-LL shows no significant changes. Overall, there is no substantial extension in drought duration across the three future periods. The pairwise comparisons among the five GCMs' TADD projections over three future periods generally demonstrated statistically significant differences ($p < 0.05$). The drought durations simulated by the two methods for PET (Fig. 5 and Supplementary Fig. 5) showed minimal difference under the SSP1-2.6 scenario. However, under SSP5-8.5, the drought durations simulated by the conventional PM-RC algorithm exhibit lower values in the early period but significantly higher in the later period compared to those estimated by the method considering vegetation-CO_2 interactions.

The total annual drought frequency (TADF) measures the frequency of drought occurrences. Figure 6 illustrates the changes in TADF. In the low-emission scenario, the drought frequency does not exhibit any significant change over the three future periods. However, in the high-emission scenario, there appears to be a trend toward a decrease in drought frequency. Overall, there is no significant shift in drought frequency over the three future periods. Pairwise comparisons among the five GCMs' TADF projections over the future three periods mostly revealed statistically significant differences ($p < 0.05$). When comparing the drought frequency derived from the simulation of the two methods for PET (Fig. 6 and Supplementary Fig. 6), it is evident that the frequencies calculated by both methods are similar, indicating minimal difference.

Trends in drought event characteristics

The analysis of TADS trends aids in determining whether the severity of droughts across China is weakening or intensifying. Figure 7 illustrates the spatial pattern of TADS trends across China. Under the SSP1-2.6 scenario, most regions of China exhibit a decreasing trend in drought severity, though this trend is not statistically significant. In contrast, under SSP5-8.5, the drought severity decreases in much of southwest China but increases significantly in central and southeast China. The significant upward trend in drought severity projected by GFDL-ESM4 under SSP1-2.6 is widely distributed. Nationwide, the drought severity projected by MPI-ESM1-2-HR under SSP5-8.5 shows a decreasing trend, though not significant. In general, future drought severity in China exhibits a significant upward trend in only a few regions and a downward trend in most regions. When comparing the drought severity trends using the two different PET estimation methods (Fig. 7 and Supplementary Fig. 7), the spatial patterns under SSP1-2.6 are similar between the methods. However, under SSP5-8.5, the trends calculated by the conventional PM-RC algorithm exhibit a more widespread and significant increase in severity.

Based on the analysis of TADD trends, the duration of droughts across China is observed to either shorten or lengthen. Figure 8 illustrates the spatial pattern of TADD trends across China. Under the SSP1-2.6 scenario, most areas in China show a trend towards shorter drought durations, though these trends are not statistically significant. Conversely, under SSP5-8.5, the duration of droughts tends to decrease in the majority of southwest China, while increasing significantly in central and southeast China. The most extensive increase in drought duration under the low-emission scenario is projected by GFDL-ESM4. In contrast, the drought duration projected by MPI-ESM1-2-HR under the high-emission scenario predominantly follows a downward trend nationwide, though not significant. In general, future drought duration in China is projected to experience a significant upward trend in only a few regions, and a downward trend in most regions. When

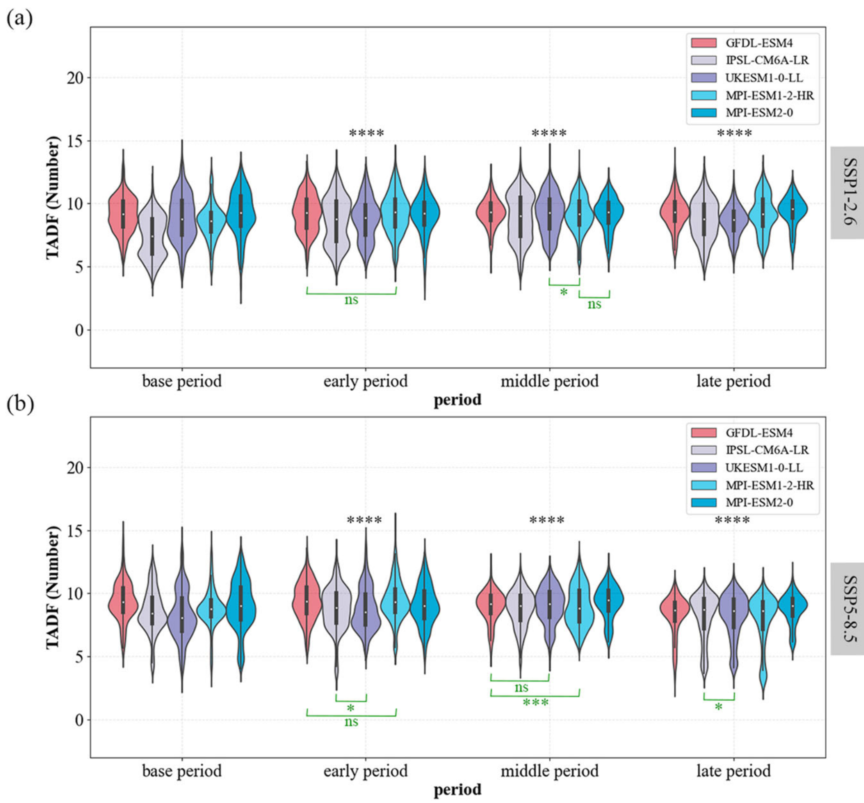

Fig. 6 Total annual drought frequency under different scenarios and time periods. TADF (PET calculated from PM-CO2) for the base period (1980–2014) and three future periods (2015–2040, 2041–2070, and 2071–2100) under **a** SSP1-2.6 and **b** SSP5-8.5. Significance levels are indicated by **** for $p \leq 0.0001$, *** for $p \leq 0.001$, ** for $p \leq 0.01$, and * for $p \leq 0.05$. The lower green sign indicates the p-value between two GCMs, and the upper **** sign represents that the p-value between all two GCMs, except the lower green one, is ≤ 0.0001.

comparing the drought duration trends using two different PET estimation methods (Fig. 8 and Supplementary Fig. 8), the spatial patterns under SSP1-2.6 are almost the same. However, under SSP5-8.5, the trends calculated using the conventional PM-RC algorithm show a more extensive distribution of significant increases in drought duration.

The analysis of TADF trends is instrumental in understanding the shifts in the frequency of future drought events. The spatial patterns of TADF trends, as projected by the five GCMs, are largely consistent (Fig. 9). Most areas in China exhibit a slight downward trend, while certain areas show a significant upward trend. When comparing drought frequency trends using two different PET estimation algorithms (Fig. 9 and Supplementary Fig. 9), under the SSP1-2.6 scenario, the spatial patterns produced by both methods are almost identical. However, under the SSP5-8.5 scenario, the drought frequency trends simulated by the conventional PM-RC algorithm tend to be more widely distributed in the areas with significant increases.

DISCUSSION

Grasping the future dynamics of drought in the context of climate change remains challenging, owing to the intricate interactions between drought and a range of climatic elements. As a result, this research delves into examining the characteristics of drought events as projected by five GCMs under three different emission scenarios. This study analyzes these projections over three future periods (2015–2040, 2041–2070, 2071–2100), utilizing the daily SPEI. Unlike the more commonly employed monthly SPEI, the daily SPEI offers a more precise depiction of short-term drought events, enhancing the accuracy of drought monitoring and assessment. This approach is widely adopted and has been validated in previous studies[20,26,50,51]. Employing the daily SPEI provides a higher temporal resolution analysis, thereby enabling a more accurate detection of short-term changes in precipitation and evapotranspiration. This is particularly beneficial for the forecasting of drought events, especially in regions prone to short-term droughts under future climate change scenarios. The availability of detailed data is essential for swiftly initiating responsive actions and timely interventions to alleviate drought, thus mitigating potential adverse effects in the future. However, it's important to acknowledge that computing daily SPEI necessitates a substantial volume of data for PET calculations, which might be constrained by data availability, particularly over shorter timescales.

The results of our study show that the bias-adjusted data from the ISIMIP3b GCMs demonstrate robust capabilities to capture historical climate change in China. This increases the fidelity of using this dataset for examining future drought conditions in China. When comparing PET values calculated using different methods, we found that the conventional PM-RC model tends to overestimate future PET, particularly in the middle and late periods under high-emission scenarios (SSP3-7.0 and SSP5-8.5). This overestimation is primarily due to the rapidly increasing CO_2 concentrations, which affect vegetation behavior and result in a decelerated growth rate of PET[29]. Under a warming climate, the increase in drought severity, duration, and frequency in China is modest[31,52]. These results are at odds with some existing studies that suggest a dramatic increase in droughts over China[53,54]. When analyzing future drought events as simulated by the two PET methods, there is almost no distinction in their characteristics under the low-emission scenario. Similarly, under the high-emission scenarios, the characteristics of drought events for the baseline, early, and middle periods also show small differences between the two methods. However, in the late period under the

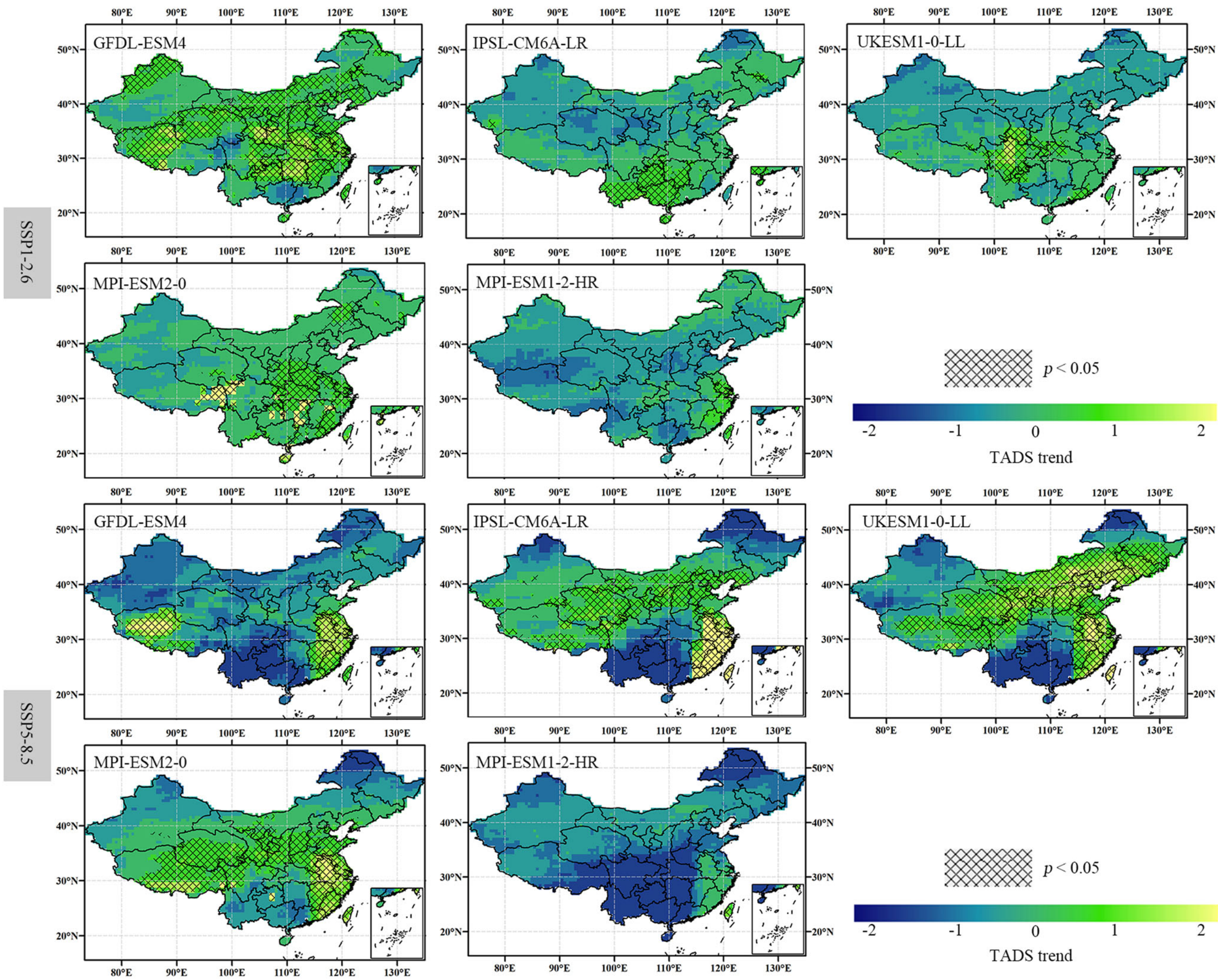

Fig. 7 Trends of TADS (PET calculated from PM-CO2) from 2015–2100 by five GCMs under two SSP scenarios (spatial pattern).

high-emission scenarios, the drought events simulated by the conventional PM-RC method are significantly more intense compared to those simulated by the method considering vegetation-CO_2 interactions.

The discrepancies are likely caused by the failure of the conventional PM-RC model to consider how vegetation responds to climate change, especially in terms of CO_2 effects. The conventional method was more suited to historical and earlier periods when CO_2 concentrations were relatively stable or slightly increasing. In contrast, during later periods, the rapidly increasing CO_2 concentrations have a substantial effect on vegetation behavior via leaf stomata and canopy structure[55,56]. High CO_2 concentrations allow plants to absorb CO_2 more efficiently, thereby reducing the frequency and duration of stomatal openings, and enhancing the plant's water use efficiency, leading to a decrease in water demand and a slower rate of evapotranspiration from the plant[57,58]. Plants regulate their water and gas exchange via stomata. In conditions of heightened CO_2, plants may reduce stomatal conductance due to more efficient carbon dioxide acquisition, which consequently leads to a reduction in water release[31,59]. The PM-CO_2 equation considers the effects of both stomata and canopy structure, offering better results than conventional models, particularly in the context of analyzing climate change impacts.

It's important to note that there are considerable differences in drought projections among the five GCMs in this study[54,60]. These differences among the GCMs can be attributed to a range of factors such as differences in model structure, parameter configurations, boundary conditions, and variations in physical and numerical schemes[38,61,62]. To enhance our understanding and clarify these discrepancies, further research and validation using observational data are crucial.

METHODS

Data collection

To project future drought conditions in China, we used the output of GCMs within the CMIP6 framework (https://esgf-node.llnl.gov/search/cmip6/, last access: Nov. 3, 2023). However, the spatial resolution of the CMIP6 output was coarse and systematically biased, prompting Lange[63] to employ a trend-holding-based parameter quantile mapping method to correct the bias and subsequently release the ISIMIP3b dataset (https://data.isimip.org/search/tree/ISIMIP3b/, last access: November 3, 2023). The ISIMIP3b comprises outputs from five GCMs: GFDL-ESM4, IPSL-CM6A-LR, MPI-ESM1-2-HR, MRI-ESM2-0, and UKESm1-0-LL. In terms of the oceanic and atmospheric modular components, these five GCMs are structurally independent, and their representation for biogeography process ranges from fair (IPSL-CM6A-

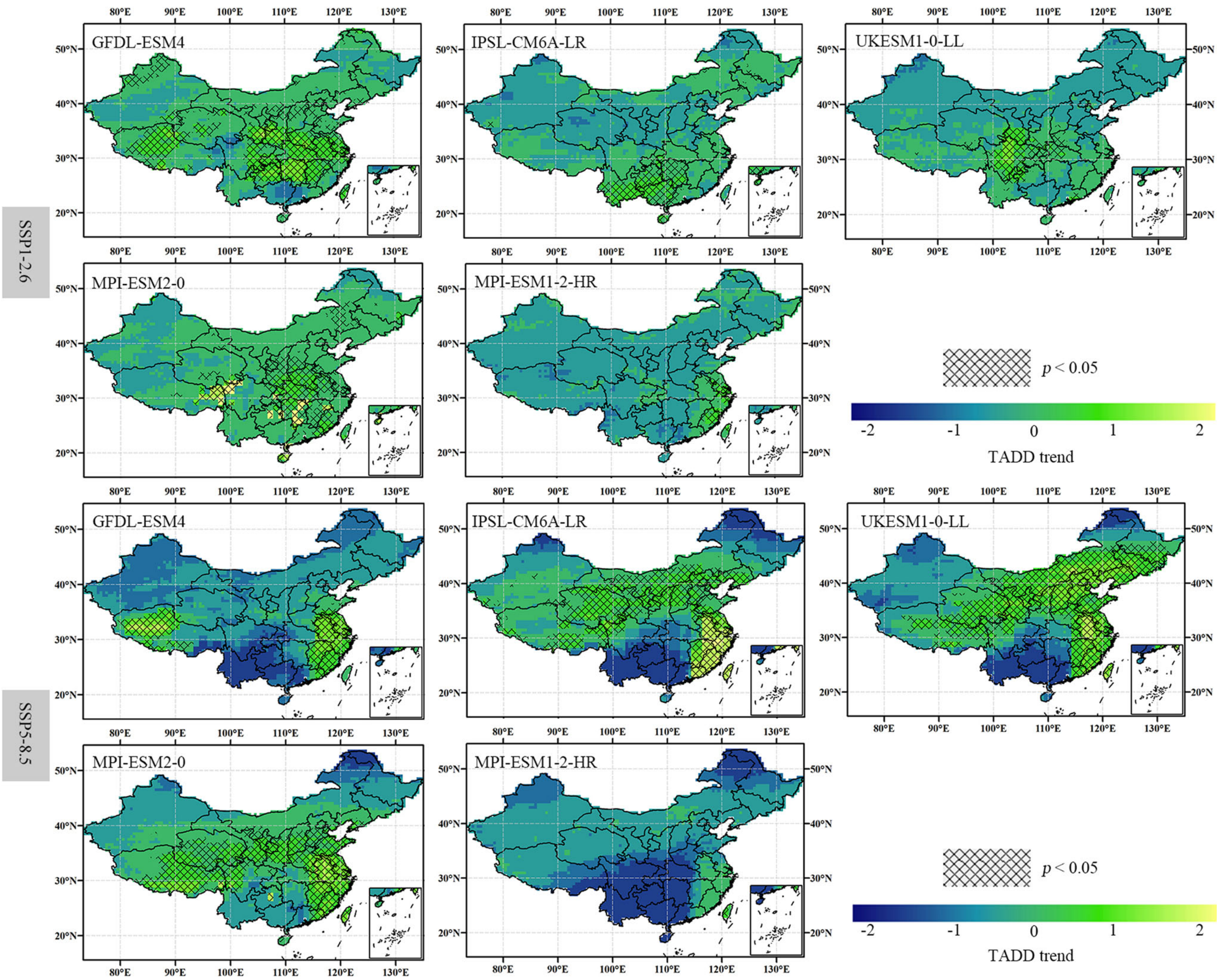

Fig. 8 Trends of TADD (PET calculated from PM-CO2) from 2015–2100 by five GCMs under two SSP scenarios (spatial pattern).

LR, and MPI-ESM1-2-HR) to good (GFDL-ESM4, and MRI-ESM2-0, UKESM1-0-LL) as indicated by informal surveys from experts involved in the Coordinated Research in Earth Systems and Climate: Experiments, kNowledge, Dissemination and Outreach (CRESCENDO) project[64,65]. Regarding climate sensitivity, the dataset encompasses three GCMs characterized by low climate sensitivity (GFDL-ESM4, MPI-ESM1-2-HR, and MRI-ESM2-0) and two GCMs with high climate sensitivity (IPSL-CM6A-LR and UKESM1-0-LL). Together, these models represent the full spectrum of climate sensitivity within the CMIP6 ensemble[66]. To investigate variations in future drought conditions in China under different emission scenarios, we used the GCMs output under three scenarios: SSP1-2.6, SSP3-7.0, and SSP5-8.5.

In this research, we gathered datasets encompassing precipitation, temperature, downward shortwave radiation, downward longwave radiation, relative humidity, and wind speed data were collected for the period from 1980 to 2100, considering three emission scenarios and five GCMs under ISMIP3b. The datasets are available at a daily temporal resolution and possess a spatial resolution of 0.5° × 0.5°. To evaluate the performance of GCMs, we used version 2.0 of WFDE5 over land merged with ERA5 over the ocean (W5E5 v2.0) dataset, used for bias adjustment in ISIMIP3b as observational data (https://data.isimip.org/search/, last access: November 3, 2023)[67]. To calculate net radiation (as detailed in Supplementary Method 1), we used uncorrected data including downward upward shortwave radiation, downward longwave radiation, upward longwave radiation, and temperature from CMIP6. Within CMIP6, CO_2 concentrations are determined by shared socioeconomic pathways (SSPs). Each SSP scenario corresponds to a specific set of CO_2 concentration pathways. To calculate PET, we compiled monthly CO_2 data from CMIP6. The use of monthly CO_2 data was due to the data availability.

Drought index calculation

We used the daily SPEI from our recent study to assess droughts[20,26,50]. The methodology for the calculation of the daily SPEI was similar to that described by Wang et al.[20]. To investigate meteorological drought in China, we computed daily SPEI for a 30-day cumulative water deficit (D), derived by subtracting PET from precipitation (P) (i.e., $D =$ P-PET)[19,68]. The SPEI series was obtained by standardizing the D series via the generalized extreme value (GEV) distribution, generally recognized as the best-suited method for calculating SPEI[22,69]. For detailed calculation procedures and additional references, please refer to Wang et al.[20] and Mann (1945). The wet and dry grading employed in this study was based on previous research[14,20,50]. In this study, we used the PM-CO_2 model (as detailed in Supplementary Method 3) to calculate PET, and for a comprehensive comparative analysis, we also used the PM-RC model (as detailed in Supplementary Method 2) to evaluate the PET and drought event characteristics of the five GCMs under

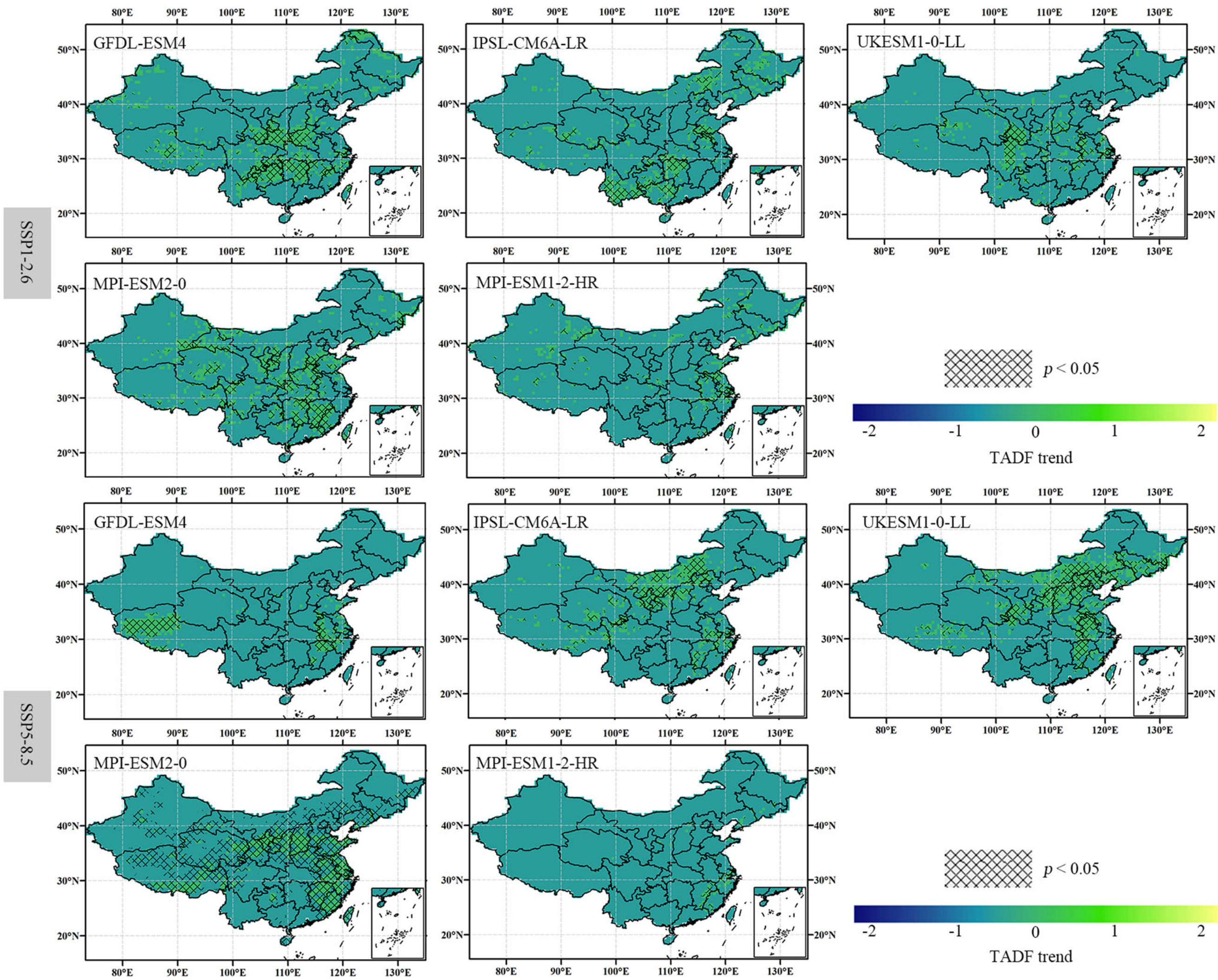

Fig. 9 Trends of TADF (PET calculated from PM-CO2) from 2015–2100 by five GCMs under two SSP scenarios (spatial pattern).

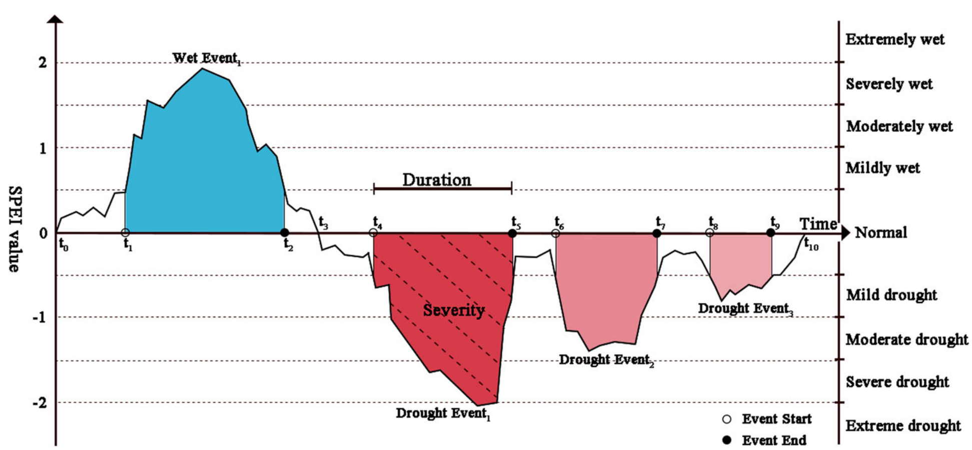

Fig. 10 Illustrative diagram of drought events and three characteristics (including severity, duration, and frequency) defined by SPEI.

the three scenarios. As the PM-RC equation was developed at a constant surface resistance (r_s) of 70 s m^{-1}, the PM-CO_2 equation may overestimate PET when plants reduce stomatal conductance and enhance water use efficiency in response to increased CO_2 concentrations[27,70]. Yang et al. (2019)[32] addressed this issue by quantifying the general sensitivity of r_s to CO_2.

Drought event identification

The run theory introduced by Evjevich (1967), was employed to identify the characteristics of drought events. The duration of a drought is defined as the number of days between the onset and the cessation of the event. The severity of drought is quantified as the integrated area between the SPEI value falling below −0.5 in absolute terms and the horizontal axis for the event's duration[20]. Drought frequency denotes the cumulative count of events occurring within a specified time. Figure 10 illustrates the definition and three characteristics of drought events.

To assess and compare drought event characteristics in China, severity, duration, and frequency were aggregated annually, yielding total annual drought severity (TADS), total annual drought duration (TADD), and total annual drought frequency (TADF), respectively[20,26]. These three metrics facilitate the comparison and analysis of drought events.

Statistical methods

We used the Taylor Diagram to evaluate the performance of the five GCMs. The Taylor Diagram is a versatile graphical tool frequently utilized in meteorology to illustrate the resemblance between models and observations[71,72]. It integrates three evaluation metrics, the correlation coefficient (CC), root mean square deviation (RMSD), and standardized deviations (SD), within a polar graph. This graphical representation facilitates a more detailed evaluation of the model's performance.

To examine significant differences in projected drought among the five GCMs across the three future periods, we employed the nonparametric Wilcoxon test. This selection was based on the fact that the attributes of the simulated drought events do not conform to a normal distribution[73]. A p-value lower than 0.05 indicates a statistically significant difference in the predicted results of the two GCMs.

To identify trends and their significance in drought event characteristics, we employed the nonparametric Mann-Kendall (MK) test. This test does not demand the data to follow a normal distribution[74] and is widely used to analyze drought time series[20,75–77]. A p-value of lower than 0.05 indicates the presence of a significant trend.

DATA AVAILABILITY

The datasets used and analyzed during the current study are available from https://doi.org/10.6084/m9.figshare.24988335 or https://doi.org/10.5061/dryad.b2rbnzsp1.

CODE AVAILABILITY

The source codes for the analysis of this study are available from https://github.com/wangqianfeng23/Daily_SPEI-main.

Received: 27 July 2023; Accepted: 18 January 2024;
Published online: 30 January 2024

REFERENCES

1. Li, Q. et al. Investigation to the relation between meteorological drought and hydrological drought in the upper Shaying River Basin using wavelet analysis. *Atmos. Res.* **234**, 104743 (2020).
2. Ukkola, A. M., De Kauwe, M. G., Roderick, M. L., Abramowitz, G. & Pitman, A. J. Robust future changes in meteorological drought in CMIP6 projections despite uncertainty in precipitation. *Geophys. Res. Lett.* **47**, e2020GL087820 (2020).
3. Leng, S. et al. Assessing the impact of extreme droughts on dryland vegetation by multi-satellite solar-induced chlorophyll fluorescence. *Remote Sens.* **14**, 1581 (2022).
4. Sun, P., Ma, Z., Zhang, Q., Singh, V. P. & Xu, C.-Y. Modified drought severity index: model improvement and its application in drought monitoring in China. *J. Hydrol.* **612**, 128097 (2022).
5. Li, Y. L., Wang, B. Y. & Gong, Y. J. Drought assessment based on data fusion and deep learning. *Comput. Intell. Neurosci.* **2022**, 4429286 (2022).
6. Kiem, A. S. et al. Natural hazards in Australia: droughts. *Clim. Change* **139**, 37–54 (2016).
7. Wang, T., Tu, X., Singh, V. P., Chen, X. & Lin, K. Global data assessment and analysis of drought characteristics based on CMIP6. *J. Hydrol.* **596**, 126091 (2021).
8. Zhang, Q. et al. Nonparametric integrated agrometeorological drought monitoring: model development and application. *J. Geophys. Res. Atmos.* **123**, 73–88 (2018).
9. Zhang, R. R., Qi, J. Y., Leng, S. & Wang, Q. F. Long-term vegetation phenology changes and responses to preseason temperature and precipitation in Northern China. *Remote Sens.* **14**, 1396 (2022).
10. Luo, D., Jin, H., Bense, V. F., Jin, X. & Li, X. Hydrothermal processes of near-surface warm permafrost in response to strong precipitation events in the Headwater Area of the Yellow River, Tibetan Plateau. *Geoderma* **376**, 114531 (2020).
11. Wang, Y. et al. Drought risk assessment of spring maize based on APSIM crop model in Liaoning province, China. *Int. J. Disaster Risk Reduct.* **45**, 101483 (2020).
12. Zeng, J. et al. Improving the drought monitoring capability of VHI at the global scale via ensemble indices for various vegetation types from 2001 to 2018. *Weather Clim. Extremes* **35**, 100412 (2022).
13. Zeng, J. et al. An improved global vegetation health index dataset in detecting vegetation drought. *Sci. Data* **10**, 338 (2023).
14. McKee, T. B., Doesken, N. J. & Kleist, J. R. The relationship of drought frequency and duration to time scales. Eighth Conference on Applied Climatology, 17–22 (1993).
15. Dai, A., Trenberth, K. E. & Qian, T. T. A global dataset of Palmer Drought Severity Index for 1870-2002: Relationship with soil moisture and effects of surface warming. *J. Hydrometeorol.* **5**, 1117–1130 (2004).
16. Wells, N., Goddard, S. & Hayes, M. J. A self-calibrating Palmer Drought Severity Index. *J. Clim.* **17**, 2335–2351 (2004).
17. Zhai, J. et al. Future drought characteristics through a multi-model ensemble from CMIP6 over South Asia. *Atmos. Res.* **246**, 105111 (2020).
18. Sharma, S. et al. Projected drought conditions over southern slope of the central Himalaya using CMIP6 models. *Earth Syst. Environ.* **5**, 849–859 (2021).
19. Vicente-Serrano, S. M., Beguería, S. & López-Moreno, J. I. A multiscalar drought index sensitive to global warming: the standardized precipitation evapotranspiration index. *J. Clim.* **23**, 1696–1718 (2010).
20. Wang, Q. F. et al. A multi-scale daily SPEI dataset for drought characterization at observation stations over mainland China from 1961 to 2018. *Earth Syst. Sci. Data* **13**, 331–341 (2021).
21. Wang, Q. et al. A comprehensively quantitative method of evaluating the impact of drought on crop yield using daily multi-scale SPEI and crop growth process model. *Int. J. Biometeorol.* **61**, 685–699 (2017).
22. Wang, Q. F. et al. The alleviating trend of drought in the Huang-Huai-Hai Plain of China based on the daily SPEI. *Int. J. Climatol.* **35**, 3760–3769 (2015).
23. Leng, S. et al. Spatiotemporal variations of dryland vegetation phenology revealed by satellite-observed fluorescence and greenness across the North Australian tropical transect. *Remote Sens.* **14**, 2985 (2022).
24. Wang, Q. et al. The effects of air temperature and precipitation on the net primary productivity in China during the early 21st century. *Front. Earth Sci.* **12**, 818–833 (2018).
25. Lu, E. et al. The day-to-day monitoring of the 2011 severe drought in China. *Clim. Dyn.* **43**, 1–9 (2013).
26. Xu, F., Bento, V. A., Qu, Y. & Wang, Q. Projections of global drought and their climate drivers using CMIP6 global climate models. *Water* **15**, 2272 (2023).
27. Maidment, D. R. *Handbook of Hydrology* (McGraw-Hill, 1993).
28. Allen, R. G., Pereira, L. S., Raes, D. & Smith, M. *Crop Evapotranspiration—Guidelines for Computing Crop Water Requirements FAO Irrigation and Drainage* Paper No. 56 (FAO, 1998).
29. Liu, Z., Wang, T. & Yang, H. Overestimated global dryland expansion with substantial increases in vegetation productivity under climate warming. *Environ. Res. Lett.* **18**, 054024 (2023).
30. Kim, D., Chun, J. A., Yeo, J.-H. & Ha, K.-J. Divergent flash drought risks indicated by evaporative stress and soil moisture projections under warming scenarios. *Environ. Res. Lett.* **18**, 094023 (2023).
31. Wang, T. & Sun, F. Socioeconomic exposure to drought under climate warming and globalization: The importance of vegetation-CO_2 feedback. *Int. J. Climatol.* **43**, 5778–5796 (2023).
32. Yang, Y., Roderick, M. L., Zhang, S., McVicar, T. R. & Donohue, R. J. Hydrologic implications of vegetation response to elevated CO_2 in climate projections. *Nat. Clim. Chang*. **9**, 44–48 (2019).
33. Li, H. et al. Drylands face potential threat of robust drought in the CMIP6 SSPs scenarios. *Environ. Res. Lett.* **16**, 114004 (2021).
34. Yu, J., Zhou, H., Huang, J. & Yuan, Y. Prediction of multi-scale meteorological drought characteristics over the Yangtze river basin based on CMIP6. *Water* **14**, 2996 (2022).
35. Li, X., Fang, G., Wen, X., Xu, M. & Zhang, Y. Characteristics analysis of drought at multiple spatiotemporal scale and assessment of CMIP6 performance over the Huaihe River Basin. *J. Hydrol. -Reg. Stud.* **41**, 101103 (2022).

36. Song, Z. et al. Assessment of meteorological drought change in the 21st century based on CMIP6 multi-model ensemble projections over mainland China. *J. Hydrol.* **601**, 126643 (2021).
37. Wang, Q. et al. Freeze-thaw cycle representation alters response of watershed hydrology to future climate change. *Catena* **195**, 104767 (2020).
38. Su, B. et al. Insight from CMIP6 SSP-RCP scenarios for future drought characteristics in China. *Atmos. Res.* **250**, 105375 (2021).
39. Cook, B. I. et al. Twenty-first century drought projections in the CMIP6 forcing scenarios. *Earth's Future* **8**, e2019EF001461 (2020).
40. Song, Y. H., Shahi, A. & Chung, E. S. Differences in multi-model ensembles of CMIP5 and CMIP6 projections for future droughts in South Korea. *Int. J. Climatol.* **42**, 2688–2716 (2022).
41. Riahi, K. et al. The shared socioeconomic pathways and their energy, land use, and greenhouse gas emissions implications: an overview. *Glob. Environ. Change-Hum. Policy Dimens.* **42**, 153–168 (2017).
42. Mishra, V., Bhatia, U. & Tiwari, A. D. Bias-corrected climate projections for South Asia from Coupled Model Intercomparison Project-6. *Sci. Data* **7**, 338 (2020).
43. Almazroui, M. et al. Projected changes in temperature and precipitation over the United States, Central America, and the Caribbean in CMIP6 GCMs. *Earth Syst. Environ.* **5**, 1–24 (2021).
44. Dosio, A. et al. Projected future daily characteristics of African precipitation based on global (CMIP5, CMIP6) and regional (CORDEX, CORDEX-CORE) climate models. *Clim. Dyn.* **57**, 3135–3158 (2021).
45. Xin, X. G., Wu, T. W., Zhang, J., Yao, J. C. & Fang, Y. J. Comparison of CMIP6 and CMIP5 simulations of precipitation in China and the East Asian summer monsoon. *Int. J. Climatol.* **40**, 6423–6440 (2020).
46. Ritchie, J. & Dowlatabadi, H. Why do climate change scenarios return to coal? *Energy* **140**, 1276–1291 (2017).
47. Ma, Z. et al. The characteristics and evaluation of future droughts across China through the CMIP6 multi-model ensemble. *Remote Sens.* **14**, 1097 (2022).
48. He, S., Chen, K., Liu, Z. & Deng, L. Exploring the impacts of climate change and human activities on future runoff variations at the seasonal scale. *J. Hydrol.* **619**, 129382 (2023).
49. Yin, J. et al. Thermodynamic driving mechanisms for the formation of global precipitation extremes and ecohydrological effects. *Earth Syst. Sci. Data* **66**, 92–110 (2022).
50. Zhang, R. R. et al. The first high spatial resolution multi-scale daily SPI and SPEI raster dataset for drought monitoring and evaluating over China from 1979 to 2018. *Big Earth Data* **7**, 860–885 (2023).
51. Wan, L. et al. Drought characteristics and dominant factors across China: Insights from high-resolution daily SPEI dataset between 1979 and 2018. *Sci. Total Environ.* **901**, 166362 (2023).
52. Jiang, H. et al. Effect of CO2 concentration on drought assessment in China. *Int. J. Climatol.* **42**, 7465–7482 (2022).
53. Zhao, R., Sun, H., Xing, L., Li, R. & Li, M. Effects of anthropogenic climate change on the drought characteristics in China: From frequency, duration, intensity, and affected area. *J. Hydrol.* **617**, 129008 (2023).
54. Xu, Y., Zhang, X., Hao, Z., Hao, F. & Li, C. Projections of future meteorological droughts in China under CMIP6 from a three-dimensional perspective. *Agric. Water Manag.* **252**, 106849 (2021).
55. Ainsworth, E. A. & Rogers, A. The response of photosynthesis and stomatal conductance to rising [CO2]: mechanisms and environmental interactions. *Plant, Cell Environ.* **30**, 258–270 (2007).
56. Vicente-Serrano, S. M. et al. Global characterization of hydrological and meteorological droughts under future climate change: the importance of time-scales, vegetation-CO2 feedbacks and changes to distribution functions. *Int. J. Climatol.* **40**, 2557–2567 (2019).
57. Kong, R. et al. Increasing sensitivity of dryland water use efficiency to soil water content due to rising atmospheric CO2. *Sci. Total Environ.* **905**, 167087 (2023).
58. Hui, D. et al. Canopy radiation- and water-use efficiencies as affected by elevated [CO2]. *Glob. Change Biol.* **7**, 75–91 (2008).
59. Hao, G.-Y. et al. Coordinated responses of plant hydraulic architecture with the reduction of stomatal conductance under elevated CO2 concentration. *Tree Physiol.* **38**, 1041–1052 (2018).
60. Schewe, J. et al. Multimodel assessment of water scarcity under climate change. *Proc. Natl Acad. Sci. USA* **111**, 3245–3250 (2014).
61. Zhang, M. et al. Spatio-temporal characteristics and driving factors of the meteorological drought across China based on CMIP6. *Hydrol. Res.* **54**, 382–400 (2023).
62. Hawkins, E. & Sutton, R. The potential to narrow uncertainty in projections of regional precipitation change. *Clim. Dyn.* **37**, 407–418 (2010).
63. Lange, S. Trend-preserving bias adjustment and statistical downscaling with ISI-MIP3BASD (v1.0). *Geosci. Model Dev.* **12**, 3055–3070 (2019).
64. Xu, X. et al. Projected seasonal changes in future rainfall erosivity over the Lancang-Mekong River basin under the CMIP6 scenarios. *J. Hydrol.* **620**, 129444 (2023).
65. Soliman, M. M., Al-Khalaf, A. A. & El-Hawagry, M. S. A. Effects of climatic change on potential distribution of *Spogostylum ocyale* (Diptera: Bombyliidae) in the Middle East using maxent modelling. *Insects* **14**, 120 (2023).
66. Stefan Lange, M. B. ISIMIP3b bias-adjusted atmospheric climate input data (v1.1). *ISIMIP Repository*, https://doi.org/10.48364/ISIMIP.842396.1 (ISIMIP Repository, 2021).
67. Stefan Lange, C. M. et al. WFDE5 over land merged with ERA5 over the ocean (W5E5 v2.0). *ISIMIP Repository*, https://doi.org/10.48364/ISIMIP.342217 (ISIMIP Repository, 2021).
68. Wang, Q. et al. Temporal-spatial characteristics of severe drought events and their impact on agriculture on a global scale. *Quat. Int.* **349**, 10–21 (2014).
69. Monish, N. T. & Rehana, S. Suitability of distributions for standard precipitation and evapotranspiration index over meteorologically homogeneous zones of India. *J. Earth Syst. Sci.* **129**, 1–19 (2019).
70. Milly, P. C. D. & Dunne, K. A. Potential evapotranspiration and continental drying. *Nat. Clim. Chang.* **6**, 946–949 (2016).
71. Mondal, S. K. et al. Doubling of the population exposed to drought over South Asia: CMIP6 multi-model-based analysis. *Sci. Total Environ.* **771**, 145186 (2021).
72. Taylor, K. E. Summarizing multiple aspects of model performance in a single diagram. *J. Geophys. Res.* **106**, 7183–7192 (2001).
73. Raje, D. Changepoint detection in hydrologic series of the Mahanadi river basin using a fuzzy Bayesian approach. *J. Hydrol. Eng.* **19**, 687–698 (2014).
74. Mann, H. B. Non-parametric tests against trend. *Econometrica* **12**, 245–259 (1945).
75. Ghosh, K. G. Analysis of rainfall trends and its spatial patterns during the last century over the Gangetic West Bengal, Eastern India. *J. Geovis. Spat. Anal.* **2**, 15 (2018).
76. Wu, X. et al. The effect of drought on vegetation gross primary productivity under different vegetation types across China from 2001 to 2020. *Remote Sens.* **14**, 4658 (2022).
77. Zhang, T., Su, X., Zhang, G., Wu, H. & Liu, Y. Projections of the characteristics and probability of spatially concurrent hydrological drought in a cascade reservoirs area under CMIP6. *J. Hydrol.* **613**, 128472 (2022).

ACKNOWLEDGEMENTS

Thanks to the National Key Research and Development Program of China [grant number [grant number 2023YFC3006604], the Natural Science Foundation of Fujian Province [grant number 2021J01627], and the National Natural Science Foundation of China [grant number 41601562] for their financial support. Thanks to Prof. Dr. Wenping Yuan, Prof. Dr. Xiuzhi Chen, Prof. Dr. Yunjun Yao, Prof. Dr. Yuting Yang, and Prof. Dr. Dalei Hao for their help in this work.

AUTHOR CONTRIBUTIONS

Conceptualization, F.X. and Q.W.; validation, Y.Q., H.S., J.Q., X.Z., J.Q., V.B., Q.W., and F.X.; formal analysis, F.X. and Q.W.; Methodology, F.X. R.Z., L.W., and Q.W.; investigation, F.X.; data curation, F.X.; writing—original draft preparation, F.X.; writing—review and editing, Y.Q., H.S., V.B., Q.W., L.W., J.Q., X.Z., J.Q., M.L., and F.X.; visualization, F.X.; supervision, V.B. and Q.W.; funding acquisition, Y.Q., and Q.W. The authors declare no competing interests.

COMPETING INTERESTS

The authors declare no competing interests.

ADDITIONAL INFORMATION

Supplementary information The online version contains supplementary material available at https://doi.org/10.1038/s41612-024-00578-5.

Correspondence and requests for materials should be addressed to Qianfeng Wang.